nature materials

LETTERS

PUBLISHED ONLINE: 6 JULY 2015 | DOI: 10.1038/NMAT4341

Spatially resolved ultrafast magnetic dynamics initiated at a complex oxide heterointerface

M. Först[1,2*†], A. D. Caviglia[3†], R. Scherwitzl[4], R. Mankowsky[1,2], P. Zubko[4‡], V. Khanna[1,5,6], H. Bromberger[1,2], S. B. Wilkins[7], Y.-D. Chuang[8], W. S. Lee[9], W. F. Schlotter[10], J. J. Turner[10], G. L. Dakovski[10], M. P. Minitti[10], J. Robinson[10], S. R. Clark[5,11], D. Jaksch[5,11], J.-M. Triscone[4], J. P. Hill[7], S. S. Dhesi[6] and A. Cavalleri[1,2,5]

Static strain in complex oxide heterostructures[1,2] has been extensively used to engineer electronic and magnetic properties at equilibrium[3]. In the same spirit, deformations of the crystal lattice with light may be used to achieve functional control across heterointerfaces dynamically[4]. Here, by exciting large-amplitude infrared-active vibrations in a $LaAlO_3$ substrate we induce magnetic order melting in a $NdNiO_3$ film across a heterointerface. Femtosecond resonant soft X-ray diffraction is used to determine the spatiotemporal evolution of the magnetic disordering. We observe a magnetic melt front that propagates from the substrate interface into the film, at a speed that suggests electronically driven motion. Light control and ultrafast phase front propagation at heterointerfaces may lead to new opportunities in optomagnetism, for example by driving domain wall motion to transport information across suitably designed devices.

In transition metal oxides, rearrangements in electronic and magnetic properties can be triggered by the application of magnetic[5] and electric fields[6], or pressure[7,8]. Switching has also been demonstrated in these materials using femtosecond optical excitation, at near-visible[9–12], mid-infrared[13–16] or terahertz[17–19] wavelengths.

Recently, selective excitation of lattice modes in the mid-infrared has been applied to complex oxide heterostructures, where the functional material can be separated from the optically excited region. By directly driving the $LaAlO_3$ substrate infrared-active modes in a $LaAlO_3/NdNiO_3$ heterostructure, an insulator–metal transition was triggered across the interface in the nickelate film[4].

Here, we apply time-resolved resonant soft X-ray diffraction (RSXD) to measure the concomitant magnetic response in the $NdNiO_3$ film, with nanometre spatial and femtosecond temporal resolution. We find evidence of inhomogeneous magnetic melting dynamics, with a melt front that propagates from the interface into the $NdNiO_3$ film at speeds of the order of, or even in excess of, the speed of sound. An insulator–metal transition initiated at the heterointerface and propagating inward, possibly locked to a wave of local octahedral distortions, is considered to explain these observations. Theoretical calculations using a model Hamiltonian indicate that itinerant charge carriers in a spin-ordered correlated electron insulator can dynamically scramble the magnetic order efficiently as they move into the film.

At about 200 K, metallic paramagnetic $NdNiO_3$ undergoes a transition into a low-temperature antiferromagnetic insulating state[20]. This electronic and magnetic phase transition is concomitant with a structural transformation from an orthorhombic (*Pbnm*) to a monoclinic ($P2_1/n$) crystal structure. The transition temperature depends on epitaxial strain[21], demonstrating sensitivity to lattice distortions.

We study a compressively strained 30-nm-thick $NdNiO_3$ film grown on a (111) $LaAlO_3$ substrate (see Methods). The low-temperature antiferromagnetic order on the Ni and Nd sublattices, shown schematically in Fig. 1a, can be observed by RSXD at the pseudo-cubic (1/4 1/4 1/4) wavevector[22]. Figure 1b shows the static photon-energy-dependent magnetic diffraction from this ordering, measured at the Ni $L_{2,3}$ edges using synchrotron radiation.

In a femtosecond RSXD experiment at a free electron laser (FEL), the sample was excited by mid-infrared pulses resonant with the highest-frequency $LaAlO_3$ substrate phonon, which is well separated in energy from equivalent phonons of the $NdNiO_3$ film (see Fig. 1c; further experimental details are given in the Methods).

Figure 1d shows the vibrationally induced intensity changes of the (1/4 1/4 1/4) diffraction peak, which reflect the dynamics of the antiferromagnetic order in the $NdNiO_3$ film. The peak intensity dropped by about 80% within 1.6 ps, and recovered on the tens of picosecond timescale. In contrast to the case of direct interband excitation, for which the antiferromagnetic peak dropped promptly[23], the 1.6 ps time constant for this initial reduction was significantly longer than the 200-fs pump pulse duration and the 250-fs time resolution of the experiment, where the latter is limited by the jitter between the FEL and the optical laser. We compare these dynamics to the time needed for the film to become metallic, as measured by the transient reflectivity in the 1–5 THz range induced by the same mid-infrared excitation (green dots in Fig. 1d)[4]. These two similar timescales, which reflect only average changes over the

[1]Max Planck Institute for the Structure and Dynamics of Matter, 22761 Hamburg, Germany. [2]Center for Free Electron Laser Science, 22761 Hamburg, Germany. [3]Kavli Institute of Nanoscience, Delft University of Technology, 2628 CJ Delft, The Netherlands. [4]Department of Quantum Matter Physics, Université de Genève, 1211 Genève, Switzerland. [5]Department of Physics, Clarendon Laboratory, University of Oxford, Oxford OX1 3PU, UK. [6]Diamond Light Source, Didcot OX11 0DE, UK. [7]Condensed Matter Physics and Materials Science Department, Brookhaven National Laboratory, Upton, New York 11973, USA. [8]Advanced Light Source, Lawrence Berkeley Laboratory, Berkeley, California 94720, USA. [9]The Stanford Institute for Materials and Energy Sciences (SIMES), Stanford Linear Accelerator Center (SLAC) National Accelerator Laboratory and Stanford University, Menlo Park, California 94025, USA. [10]Linac Coherent Light Source, Stanford Linear Accelerator Center (SLAC) National Accelerator Laboratory, Menlo Park, California 94025, USA. [11]Centre for Quantum Technologies, National University of Singapore, Singapore 117543, Singapore. †These authors contributed equally to this work. ‡Present address: London Centre for Nanotechnology and Department of Physics and Astronomy, University College London, London WC1H 0AH, UK. *e-mail: michael.foerst@mpsd.mpg.de

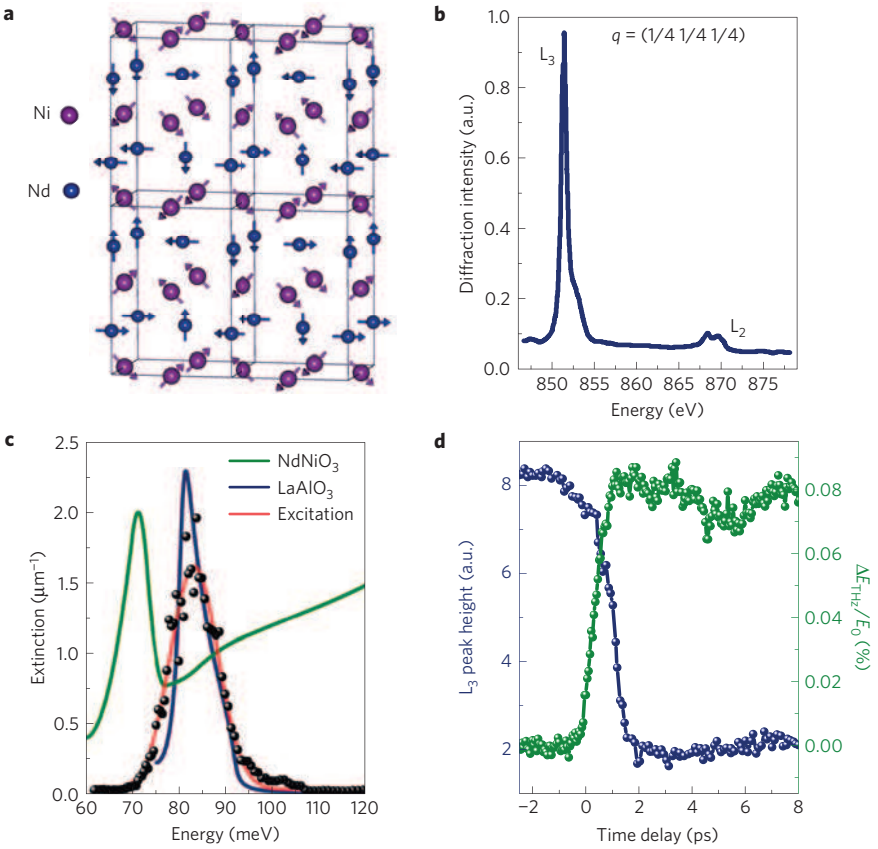

Figure 1 | Magnetic ordering in $NdNiO_3$ and the vibrationally induced phase transition. a, Visualization of the complex antiferromagnetic ordering in $NdNiO_3$. **b**, Energy scan of the (1/4 1/4 1/4) diffraction peak, associated with the magnetic order on the Ni sublattice, around the Ni $L_{2,3}$ edges. These data were measured on the $NdNiO_3/LaAlO_3$ heterostructure at 15 K. **c**, Wavelength-dependent inverse penetration depth of mid-infrared light around the $NdNiO_3$ (green) and $LaAlO_3$ (blue) high-frequency phonon resonances. The energy spectrum of the excitation pulses at 15 μm wavelength (black data points, fitted by a Gaussian profile in red) is tuned into resonance with the substrate mode. **d**, The blue data points show changes of the peak intensity of the Ni L_3 diffraction peak at 852 eV, following this optical excitation with a fluence of 4 mJ cm^{-2}. The green data points show the transient terahertz reflectivity of an equivalent sample under identical excitation conditions. The melting of the magnetic order and the insulator–metal transition both take place on the same timescale.

whole film, suggest a connection between the insulator-to-metal transition and the melting of magnetic order.

In Fig. 2, we plot the transient θ–2θ scans for the (1/4 1/4 1/4) diffraction peak, sensitive to the out-of-plane antiferromagnetic ordering. In equilibrium, that is, at negative time delay, a narrow diffraction peak and Laue oscillations are observed, indicating that magnetic order is homogeneous across the entire film, with sharp magnetic boundaries.

Figure 2 further shows that a significant peak broadening and a suppression of the Laue oscillations accompany the photoinduced reduction in peak intensity. The broadening of the diffraction peak implies that the excitation melts the magnetic order only over a fraction of the film. The suppression of the Laue oscillations indicates that the boundary between the ordered and disordered regions of the film is not sharp.

Note that throughout these dynamics the in-plane correlation length, as measured by transverse rocking curves (θ scans), remains unchanged (see Supplementary Information). Hence, the dynamics discussed here are one-dimensional, evolving along the sample growth direction.

The spatial distribution of the magnetic order at a time delay τ was analysed quantitatively with the following expression for kinematic diffraction

$$I_\tau(q) \propto \left| \int_0^D F(z,\tau) e^{-iqz} dz \right|^2 \quad (1)$$

Here, the magnetic profile is represented by the space- and time-dependent structure factor $F(z,\tau)$, where $q = 4\pi \sin\theta/\lambda$ is the magnitude of the scattering wavevector (with θ being the diffraction angle and λ the X-ray wavelength), z is the distance into the film, and D is the film thickness.

Previous work has shown that these complex dynamics are initiated at the buried interface[4]. Also, the transient θ–2θ scans show that the fraction of material, which is melted, increases with time, and that the order–disorder interface becomes progressively smeared in time. Hence, we chose a functional form $F(z,\tau)$ that describes a soliton-like demagnetization front, propagating from the heterointerface into the thin film with a smeared and adjustable phase front:

$$F(z,\tau) = F_0 \left(\frac{1}{2} + \frac{1}{2} \mathrm{erf}\left(\frac{z - z_f(\tau)}{d_f(\tau)} \right) \right) \quad (2)$$

In this case, F_0 is the equilibrium structure factor, and z_f and d_f are the time-dependent position and width of that phase front separating the unperturbed antiferromagnetic order from the disordered region of the film. Numerical fits of equations (1) and (2) to the diffraction peak at selected time delays are shown as red solid lines in the lower panel of Fig. 2 and give excellent agreement with the data.

Figure 3b shows the corresponding early timescale evolution of the space-dependent magnetic order, represented as $|F(z,\tau)|^2$. At negative time delays, the $NdNiO_3$ film is homogeneously ordered,

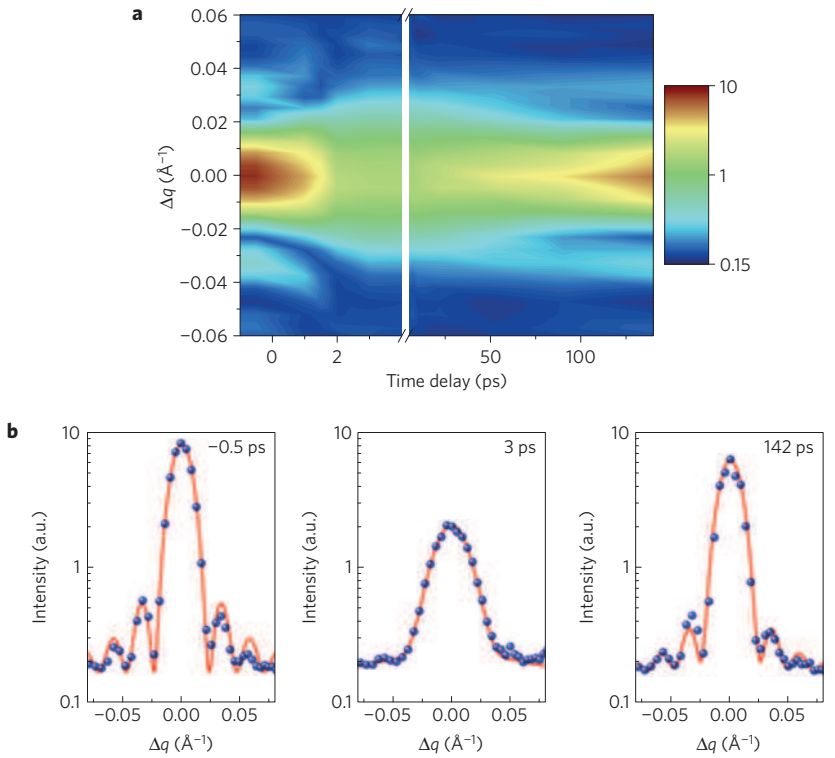

Figure 2 | Temporal evolution of the antiferromagnetic order in reciprocal space. a, Lattice-induced dynamics of the momentum dependence of the (1/4 1/4 1/4) Ni L_3-edge diffraction peak (θ–2θ scans), on both short and long timescales. The diffraction intensity is colour-coded on a logarithmic scale. **b**, The same diffraction peak at selected time delays before and after the mid-infrared excitation (blue dots), overlaid with numerical fits (red lines) that assume a heterogeneous melting of the antiferromagnetic order triggered at the $NdNiO_3/LaAlO_3$ interface as described in the text.

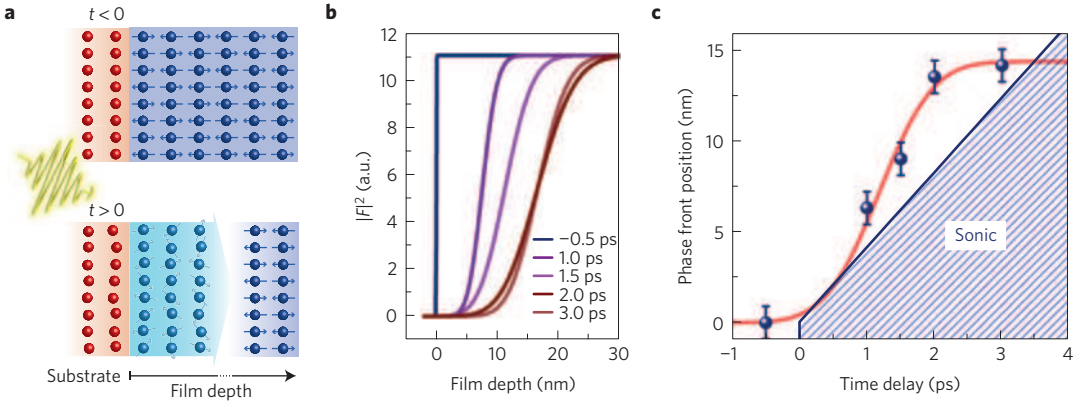

Figure 3 | Real-space dynamics of the antiferromagnetic order. a, Schematic illustration of the demagnetization process. At negative time delay, the $NdNiO_3$ film is homogeneously ordered. Direct excitation of a substrate phonon triggers a magnetic melt front, propagating from the interface into the film. **b**, Short-timescale spatial dynamics of the magnetic order along the [111] direction, extracted from the numerical fits to the diffraction peaks shown in Fig. 2. **c**, Centre position of the phase front, separating the melted from the unperturbed region of the film as defined in equation (2) (blue dots). The error bars are the standard errors obtained from the fits. The red solid line is a guide to the eye. The striped area marks the sonic regime, given by the 4.1×10^3 m s^{-1} $NdNiO_3$ longitudinal speed of sound extracted from acoustic echo times in ref. 24.

with a sharp boundary at the heterointerface. The mid-infrared excitation induces heterogeneous melting, with a demagnetizing phase front that propagates halfway into the film—before coming to a stop at ~2 ps time delay. This phase front leaves a magnetically disordered region behind. The time-dependent position of the phase front z_f is plotted in Fig. 3c, which suggests that the magnetic melt front propagates at a speed of the order of, or even faster than the longitudinal sound velocity measured in a $NdNiO_3$ film[24].

The re-magnetization dynamics are shown in Fig. 4. About 10 ps after excitation, the demagnetized part of the film starts recovering. Here, the phase front begins shifting back towards the substrate interface, and at the same time the domain boundary broadens further.

The heterogeneous dynamics discussed above are unique to the mid-infrared excitation of the substrate lattice. Near-infrared illumination of the same heterostructure at 800-nm wavelength, which involves significant homogeneous charge excitation in the nickelate film[23], shows that in this case the magnetic order is uniformly melted over the entire film. This can be clearly deduced from Fig. 5a,b unveiling that the 800-nm excitation reduces the

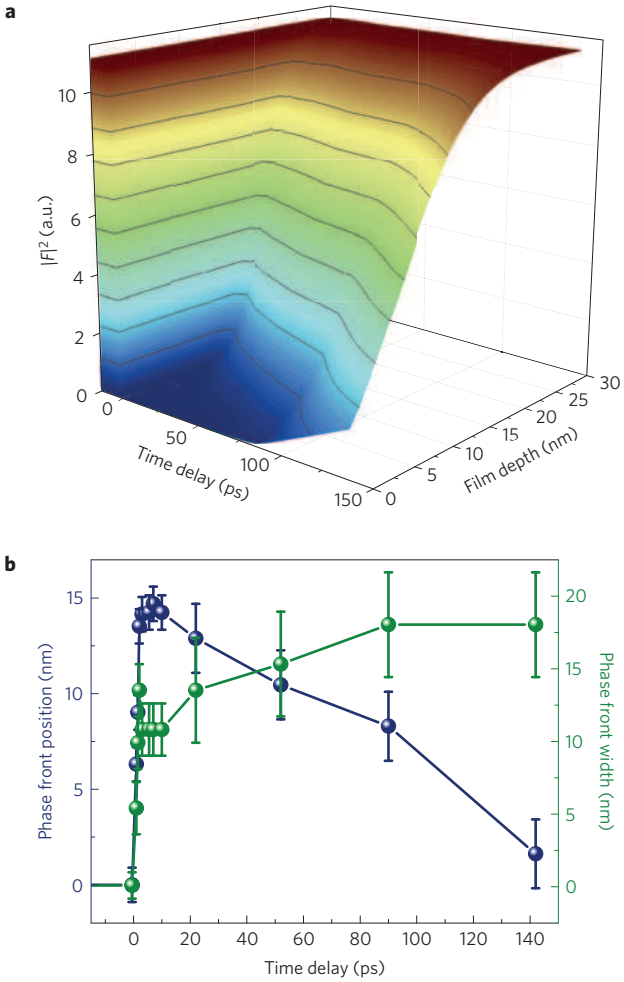

Figure 4 | Recovery dynamics of the antiferromagnetic order. **a**, Long-timescale spatial dynamics of the magnetic order along the [111] direction, extracted from the numerical fits to the diffraction peaks (shown in Fig. 2) at various time delays. **b**, Time-dependent position and width of the magnetic phase front corresponding to the data shown in panel **a**. The error bars are the standard errors obtained from the fits to the diffraction peaks (shown in Fig. 2).

intensity of the magnetic (1/4 1/4 1/4) diffraction peak and of the Laue oscillations, without any noticeable change in the peak width. An analogous fitting procedure as applied above for the mid-infrared substrate excitation (see also the red solid lines in Fig. 5b) shows the uniform and instantaneous decrease of the magnetic order across the whole film thickness.

We next turn to a discussion of the possible physical mechanisms underlying these observations. First, we can exclude direct absorption of the mid-infrared pump pulse in the nickelate film as being responsible for the observed magnetization dynamics. This is not only because the energy deposited in the nickelate is negligible (3% of the incident energy), but also because the 1-μm penetration depth in $NdNiO_3$ would imply homogeneous excitation. Note further that a uniform decrease of the magnetic order is observed when heating the $NdNiO_3$ film up to the phase transition temperature. Second, as the speed of the magnetic melt front is as high as or higher than the nominal longitudinal sound velocity[24], this cannot be caused by heat propagation, which is significantly slower. As a third possibility, one could consider a structural phase transition triggered at the buried interface, propagating inward and driving the magnetic melt front. However, a structural phase front propagates far slower than the speed of sound and is therefore also an unlikely explanation[25]. Finally, a propagating acoustic wave is also unlikely, as it is not clear how the resonant excitation of an optical phonon could initiate a propagating strain pulse on this short timescale. Note also that the strain extracted from the shift in the diffraction peak is never larger than 10^{-3}.

We propose that the direct excitation of the infrared-active substrate phonon mode induces octahedral distortions[26–28] across the interface, to locally act on the electronic and magnetic ordering of the nickelate film. Indeed, similar scenarios have been predicted for perovskite heterostructures in the static case[29]. Propagation of the phase would then presumably be driven by electronic rather than magnetic effects. We note that the anisotropic magnetic interaction stabilizing the Néel order introduces a spin gap and hence flattens the dispersion of magnons (see Supplementary Information for details), resulting in a reduced group velocity and magnon localization.

We believe that charge carriers, which are made mobile at the interface and are very efficient at randomizing spin correlations[30], are more likely to drive the magnetic front. As these itinerant carriers acquire kinetic energies that exceed magnetic energy scales, these can sustain a front that propagates. The scrambling of antiferromagnetic order would transfer initial kinetic energy into the magnetic sector[31], eventually leading to a stalling of the phase front. Although a mechanistic description of this process requires material-specific calculations, which are beyond the scope of the present paper, a model Hamiltonian description, in which charges are freed at the interface and are made mobile and diffuse into the film, confirms these qualitative arguments (see Supplementary Information). This scenario would also be compatible with the similar timescales observed for the insulator–metal transition and the magnetic order melting presented in Fig. 1d.

In summary, we have shown that the dynamics of magnetic disordering in complex oxide heterostructures follow distinctly new physical pathways when the substrate lattice is excited. We demonstrate that magnetic melting is initiated at the buried interface and propagates into the film at speeds of the order of or higher than the speed of sound. We assign the underlying physics to an electronic itinerancy front, which carries spin disordering and possibly local lattice distortions. The ability to control such ultrafast magnetic phase fronts with light may be conducive to new applications in optomagnetic devices, in which information may be encoded and shuttled in domain walls at faster rates than more established spin-torque-driven walls[32].

Methods

Methods and any associated references are available in the online version of the paper.

Received 19 March 2014; accepted 1 June 2015; published online 6 July 2015

References

1. Haeni, J. H. *et al.* Room-temperature ferroelectricity in strained $SrTiO_3$. *Nature* **430,** 758–761 (2004).
2. Lee, J. H. *et al.* A strong ferroelectric ferromagnet created by means of spin–lattice coupling. *Nature* **466,** 954–958 (2010).
3. Hwang, H. Y. *et al.* Emergent phenomena at oxide interfaces. *Nature Mater.* **11,** 103–113 (2012).
4. Caviglia, A. D. *et al.* Ultrafast strain engineering in complex oxide heterostructures. *Phys. Rev. Lett.* **108,** 136801 (2012).
5. Tomioka, Y., Asamitsu, A., Kuwahara, H., Moritomo, Y. & Tokura, Y. Magnetic-field-induced metal–insulator phenomena in $Pr_{1-x}Ca_xMnO_3$ with controlled charge-ordering instability. *Phys. Rev. B* **53,** R1689–R1692 (1996).
6. Asamitsu, A., Tomioka, Y., Kuwahara, H. & Tokura, Y. Current switching of resistive states in magnetoresistive manganites. *Nature* **388,** 50–52 (1997).
7. Hwang, H. Y., Cheong, S.-W., Radaelli, P. G., Marezio, M. & Batlogg, B. Lattice effects on the magnetoresistance in doped $LaMnO_3$. *Phys. Rev. Lett.* **75,** 914–917 (1995).

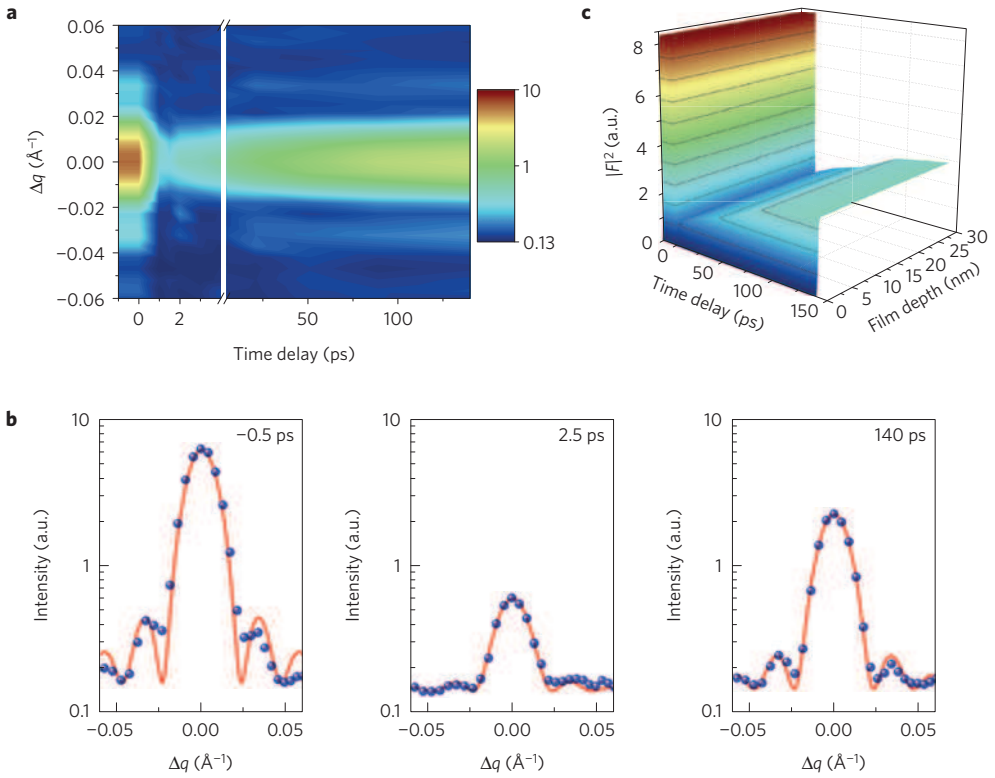

Figure 5 | Magnetization dynamics following Ni charge transfer excitation at 800 nm. a, Photoinduced dynamics of the (1/4 1/4 1/4) Ni L_3-edge diffraction peak in reciprocal space, with the diffraction intensity colour-coded on a logarithmic scale. The excitation fluence is about 4 mJ cm^{-2}. **b**, The same diffraction peak at selected time delays before and after the near-infrared excitation (blue dots), together with numerical fits (red solid lines) as described in the text. **c**, Spatial dynamics of the magnetic order along the [111] direction (extracted from these fits), showing homogeneous photoinduced demagnetization.

8. Canfield, P. C., Thompson, J. D., Cheong, S.-W. & Rupp, L. W. Extraordinary pressure dependence of the metal-to-insulator transition in the charge-transfer compounds $NdNiO_3$ and $PrNiO_3$. *Phys. Rev. B* **47,** 12357–12360 (1993).
9. Miyano, K., Tanaka, T., Tomioka, Y. & Tokura, Y. Photoinduced insulator-to-metal transition in a perovskite manganite. *Phys. Rev. Lett.* **78,** 4257–4260 (1997).
10. Cavalleri, A. *et al.* Femtosecond structural dynamics in VO_2 during an ultrafast solid–solid phase transition. *Phys. Rev. Lett.* **87,** 237401 (2001).
11. Perfetti, L. *et al.* Time evolution of the electronic structure of 1T-TaS_2 through the insulator–metal transition. *Phys. Rev. Lett.* **97,** 067402 (2006).
12. Johnson, S. L. *et al.* Femtosecond dynamics of the collinear-to-spiral antiferromagnetic phase transition in CuO. *Phys. Rev. Lett.* **108,** 037203 (2012).
13. Rini, M. *et al.* Control of the electronic phase of a manganite by mode-selective vibrational excitation. *Nature* **449,** 72–74 (2007).
14. Först, M. *et al.* Driving magnetic order in a manganite by ultrafast lattice excitation. *Phys. Rev. B* **84,** 241104R (2011).
15. Fausti, D. *et al.* Light-induced superconductivity in a stripe-ordered cuprate. *Science* **331,** 189–191 (2011).
16. Hu, W. *et al.* Optically enhanced coherent transport in $YBa_2Cu_3O_{6.5}$ by ultrafast redistribution of interlayer coupling. *Nature Mater.* **13,** 705–711 (2014).
17. Dienst, A. *et al.* Bi-directional ultrafast electric-field gating of interlayer charge transport in a cuprate superconductor. *Nature Photon.* **5,** 485–488 (2011).
18. Kampfrath, T. *et al.* Coherent terahertz control of antiferromagnetic spin waves. *Nature Photon.* **5,** 31–34 (2011).
19. Liu, M. K. *et al.* Terahertz-field-induced insulator-to-metal transition in vanadium dioxide metamaterial. *Nature* **487,** 345–348 (2012).
20. Catalan, G. Progress in perovskite nickelate research. *Phase Transit.* **81,** 729–749 (2008).
21. Catalan, G., Bowman, R. M. & Gregg, J. M. Metal–insulator transitions in $NdNiO_3$ thin films. *Phys. Rev. B* **62,** 7892–7900 (2000).
22. Scagnoli, V. *et al.* Induced noncollinear magnetic order of Nd^{3+} in $NdNiO_3$ observed by resonant soft x-ray diffraction. *Phys. Rev. B* **77,** 115138 (2008).
23. Caviglia, A. D. *et al.* Photoinduced melting of magnetic order in the correlated electron insulator $NdNiO_3$. *Phys. Rev. B* **88,** 220401 (2013).
24. Ruello, P., Zhang, S., Laffez, P., Perrin, B. & Gusev, V. Laser-induced coherent acoustical phonons mechanisms in the metal–insulator transition compound $NdNiO_3$: Thermal and nonthermal processes. *Phys. Rev. B* **79,** 094303 (2009).
25. Sokolowski-Tinten, K., Bialkowski, J., Boing, M., Cavalleri, A. & von der Linde, D. Thermal and non-thermal melting of gallium arsenide after femtosecond laser excitation. *Phys. Rev. B* **58,** R11805–R11808 (1998).
26. Först, M. *et al.* Nonlinear phononics as an ultrafast route to lattice control. *Nature Phys.* **7,** 854–856 (2011).
27. Först, M. *et al.* Displacive lattice excitation through nonlinear phononics viewed by femtosecond X-ray diffraction. *Solid State Commun.* **169,** 24–27 (2013).
28. Subedi, A., Cavalleri, A. & Georges, A. Theory of nonlinear phononics for coherent light control of solids. *Phys. Rev. B* **89,** 220301 (2014).
29. He, J., Borisevich, A., Kalinin, S. V., Pennycook, S. J. & Pantelidis, S. T. Control of octahedral tilts and magnetic properties of perovskite oxide heterostructures by substrate symmetry. *Phys. Rev. Lett.* **105,** 227203 (2010).
30. Brinkman, W. F. & Rice, T. M. Single-particle excitations in magnetic insulators. *Phys. Rev. B* **2,** 1324–1338 (1970).
31. Buleavskii, L. N., Nagaev, E. L. & Khomskii, D. I. A new type of auto-localized state of a conduction electron in an antiferromagnetic semiconductor. *Sov. Phys. JETP* **27,** 836–838 (1968).
32. Parkin, S. P., Hayashi, M. & Thomas, L. Magnetic domain-wall racetrack memory. *Science* **320,** 190–194 (2008).

Acknowledgements

We thank A. Frano for helpful discussions. Portions of this research were carried out on the SXR Instrument at the Linac Coherent Light Source (LCLS), a division of SLAC National Accelerator Laboratory and an Office of Science user facility operated by Stanford University for the US Department of Energy. The SXR Instrument is financially supported by a consortium whose membership includes the LCLS, Stanford University through the Stanford Institute for Materials Energy Sciences (SIMES), Lawrence Berkeley National Laboratory (LBNL, contract No. DE-AC02-05CH11231), University of Hamburg through the BMBF priority program FSP 301, and the Center for Free Electron Laser Science (CFEL). The research leading to these results has received financial support from the European Research Council under the European Union's Seventh Framework Programme (FP7/2007-2013)/ERC Grant Agreement no. 319286 (Q-MAC) and

no. 281403 (FEMTOSPIN). Work performed at SIMES was further supported by US Department of Energy, Office of Basic Energy Science, Division of Materials Science and Engineering, under Contract No. DE-AC02-76SF00515. Work at Brookhaven National Laboratory was financially supported by the Department of Energy, Division of Materials Science and Engineering, under contract No. DE-AC02-98CH10886.

Author contributions

A.D.C., M.F. and A.C. conceived this project. M.F., A.D.C., R.M., V.K., S.B.W., S.S.D. and J.P.H. performed the experiment at the LCLS, supported by W.F.S., J.J.T. and G.L.D. (beamline), M.P.M. and J.R. (laser), Y.-D.C. and W.S.L. (experimental endstation). The sample was grown by R.S., P.Z. and J.-M.T. M.F. and A.D.C. analysed the data with help from H.B. S.R.C. and D.J. provided the model Hamiltonian theory. M.F., A.D.C. and A.C. wrote the manuscript, with feedback from all co-authors.

Additional information

Supplementary information is available in the online version of the paper. Reprints and permissions information is available online at www.nature.com/reprints.
Correspondence and requests for materials should be addressed to M.F.

Competing financial interests

The authors declare no competing financial interests.

Methods

The $NdNiO_3$ thin film was deposited on the (111) $LaAlO_3$ single-crystal substrate by off-axis radiofrequency magnetron sputtering[33]. This substrate provides 0.5% compressive strain to the material and reduces the metal–insulator-transition temperature from a bulk value of 200 K to about 130 K for the chosen film thickness.

The static RSXD data, presented in Fig. 1b, were taken at the I06 beamline of the Diamond Light Source synchrotron X-ray source.

Femtosecond RSXD experiments were carried out at the SXR beamline of the Linac Coherent Light Source free electron laser[34]. The excitation pulses of 200-fs duration were tuned to 15 μm wavelength (82 meV photon energy) and focused onto the sample with a fluence of 4 mJ cm^{-2}. The sample was mounted onto an in-vacuum diffractometer[35] and cooled to 40 K, that is, into the antiferromagnetic insulating state. The FEL, which operated at 120 Hz repetition rate, was tuned to the 852 eV Ni L_3 edge. The bandwidth of the X-ray pulses was reduced to below 1 eV by a grating monochromator. Diffracted X-rays were detected as function of the time delay relative to the mid-infrared excitation pulses. An avalanche photodiode enabled pulse-to-pulse normalization of the diffracted to the incident light intensity.

References

33. Scherwitzl, R. *et al.* Electric-field control of the metal–insulator transition in ultrathin $NdNiO_3$ films. *Adv. Mater.* **22,** 5517–5520 (2010).
34. Schlotter, W. F. *et al.* The soft x-ray instrument for materials studies at the linac coherent light source x-ray free-electron laser. *Rev. Sci. Instrum.* **83,** 043107 (2012).
35. Doering, D. *et al.* Development of a compact fast CCD camera and resonant soft x-ray scattering endstation for time-resolved pump–probe experiments. *Rev. Sci. Instrum.* **82,** 073303 (2011).